

# Structural Studies of Anomalous Behavior in the Silica–Alumina Gel System

Susan L. Hietala\* and Douglas M. Smith\*

UNM/NSF Center for Micro-Engineered Ceramics, The University of New Mexico, Albuquerque, New Mexico 87131

C. Jeffrey Brinker\*\* and Alan J. Hurd†

Sandia National Laboratories, Albuquerque, New Mexico 87185

Altaf H. Carim\*

UNM/NSF Center for Micro-Engineered Ceramics, The University of New Mexico, Albuquerque, New Mexico 87131

Neal Dando

Alcoa Technical Center, Alcoa Center, Pennsylvania 15069

This paper compares the structure of  $\text{Al}_2\text{O}_3$ – $\text{SiO}_2$  xerogels prepared with  $\text{Al}_2\text{O}_3$  contents ranging from 21 to 75 wt% (13 to 64 mol%). The 47 wt%  $\text{Al}_2\text{O}_3$  xerogel ( $\text{Al}/\text{Si} \approx 1$ ) exhibits anomalously low surface area ( $\approx 1 \text{ m}^2/\text{g}$ ) and skeletal density compared with other  $\text{Al}_2\text{O}_3$ – $\text{SiO}_2$  compositions. Based on the results of nitrogen adsorption/condensation, helium displacement, high-resolution transmission electron microscopy (HRTEM), small-angle X-ray scattering (SAXS), and small-angle neutron scattering (SANS), we attribute the low surface area and skeletal density (density of the solid phase which is inaccessible to helium) to the formation of closed micropores, whereas the higher surface area materials exhibit a slightly coarser texture comprising open pores with radii of  $\approx 1 \text{ nm}$ . X-ray diffraction (XRD) and  $^{29}\text{Si}$  and  $^{27}\text{Al}$  magic-angle spinning nuclear magnetic resonance (MASNMR) indicate no anomalous behavior in the 47% sample on molecular length scales. HRTEM indicates the presence of a small fraction of crystallites which is supported by the SAXS results, but it is unknown if this crystallinity is related to low surface area. Low-field  $^1\text{H}$  NMR spin-lattice relaxation measurements show that the physical structure of all of the “wet” gels is similar implying that pore closure occurs during drying. Consistent with this idea, gel surface area and density increased significantly when the pore fluid (water) was replaced with a lower surface tension fluid (formamide, dioxane, ethanol, water/surfactant). [Key words: gels, characterization, silica, alumina, structure.]

## I. Introduction

IN AN earlier paper,<sup>1</sup> it was noted that the surface areas of a  $\text{SiO}_2$ – $\text{Al}_2\text{O}_3$  xerogel decreased by 2 orders of magnitude over a narrow range of composition. This anomalous effect was observed in the vicinity of 47 wt%  $\text{Al}_2\text{O}_3$  and had not been reported in previous investigations of the  $\text{SiO}_2$ – $\text{Al}_2\text{O}_3$  system.<sup>2–9</sup> In conjunction with the lower surface areas, the skeletal density measured by helium displacement was significantly lower than that observed for compositions bordering the region of this anomalous behavior. This low surface area/density behavior was observed to persist to temperatures exceeding 1073 K.

Although powders were produced in the initial work, a similar sol–gel–processing scheme could be useful for coatings. Low surface area/low skeletal density coatings are of great interest for applications such as protective coatings (thermal, chemical, etc.), hermetic seals, and low dielectric constant surface layers.

Since this anomalous surface area/skeletal density behavior is attributed to the formation of closed porosity,<sup>1</sup> several questions arise. Can direct evidence of closed porosity be obtained? How does the closed porosity evolve, and why is it observed over such a narrow  $\text{SiO}_2/\text{Al}_2\text{O}_3$  composition range? If the mechanism of pore closure is understood, the possibility exists that the effect could be reproduced in other ceramic systems. In this paper, we attempt to address these issues.

## II. Experimental Procedure

### (1) Synthesis of $\text{Al}_2\text{O}_3$ – $\text{SiO}_2$

The  $\text{Al}_2\text{O}_3$ – $\text{SiO}_2$  gels were synthesized using a sol–gel process. The  $\text{SiO}_2$  sol was prepared by adding 1 part (by volume) of tetraethyl orthosilicate (TEOS) to 2 parts (by volume) distilled water adjusted to pH 2 with hydrochloric acid. The sol, which had a molar ratio of water:TEOS of  $\approx 25:1$ , was allowed to react overnight at 298 K with stirring. No alcohol was used, but sufficient ethanol was produced during TEOS hydrolysis to result in a homogeneous sol. A saturated solution of aluminum nitrate (molar ratio of water to aluminum of  $\approx 33:1$ ) was added to the stirring sol, and 2*N* ammonium hydroxide (molar ratio of hydroxide:nitrate of  $\approx 3:1$ ) was then added to form the hydrogel at pH 6.

L. Klein—contributing editor

Manuscript No. 198118. Received September 22, 1989; approved June 11, 1990.

Supported in part by UNM/NSF Center for Micro-Engineered Ceramics (CMEC) (CMEC is supported by NSF Grant No. CDR-8803512, Los Alamos and Sandia National Laboratories, the New Mexico Research and Development Institute, and the ceramics industry.) and by NSF, NASA, DOE–BES, and the State of New Mexico.

\*Member, American Ceramic Society.

†Division 1846.

‡Division 1152.

A series of washing steps was necessary to eliminate ammonium nitrate from the hydrogel. The gel was slurried with 10 volumes of distilled water for 1 h, then centrifuged. Filter paper<sup>7</sup> was used to filter the gel, which was washed twice with distilled water before drying at 383 K overnight. The xerogel was ground with a mortar and pestle and washed with distilled water for 1 h. Filter paper<sup>8</sup> was used to filter the xerogel, and the powder was dried at 383 K overnight. Before measuring the properties of the xerogels, the powders were heated in a tube furnace at 673 K for 3 h in an air atmosphere. To investigate the effect of pore fluid, some samples were repeatedly washed with either ethanol, formamide, dioxane, or a mixture of water and a surfactant<sup>9</sup> before drying.

## (2) Characterization

Elemental analysis was determined using an X-ray fluorescence spectrometer\*\* (rhodium target with end window, 50 kV, 45 mA). Crystalline phases were identified by X-ray diffraction (XRD) using a powder X-ray diffractometer.<sup>††</sup> Nitrogen adsorption at 77 K was measured for five relative pressures in the range of 0.05 to 0.30 using an adsorption analyzer.<sup>‡‡</sup> Surface areas were calculated using the BET equation and a molecular cross-sectional area of 0.162 nm<sup>2</sup>. Before analysis, samples were outgassed at ≈383 K under vacuum for 3 h. Pore volume was estimated from the nitrogen uptake at  $P/P_0 \approx 0.99$ . Skeletal density was measured via helium displacement at ≈298 K using a micropycnometer.<sup>§§</sup> The morphology of the material was initially examined using a side-entry transmission electron microscope (TEM)<sup>¶¶</sup> at an accelerating voltage of 200 kV. A TEM<sup>\*\*\*</sup> operated at 300 kV (point-to-point resolution ≤0.20 nm) was used to further investigate the microstructure of the powders. Samples were prepared by sprinkling powder particles onto copper grids that had previously been coated with a thin carbon film.

To probe the development of pore structure during gel drying, low-field nuclear magnetic resonance (NMR) spin-lattice relaxation measurements of pore fluid were conducted. The spin-lattice relaxation time of a fluid contained in a pore,  $T_1$ , is a function of the pore size (i.e., for smaller pore sizes, a fluid will relax faster). Glaves and co-workers<sup>10</sup> have used this approach to measure changes in both total surface area and pore-size distribution during the drying of aged, base-catalyzed silica gels. If relaxation behavior is exponential (i.e., a fairly narrow, unimodal pore-size distribution), the calculated average of  $T_1$  ( $T_{1ave}$ ) is related to the  $T_1$  of the bulk fluid,  $T_{1b}$ , to the surface area of the gel,  $A_s$ , to the mass of solid sample per volume of pore fluid,  $M_v$ , and to the surface relaxation time,  $T_{1s}$ , by

$$1/T_{1ave} = 1/T_{1b} + M_v A_s / T_{1s} \quad (1)$$

During drying,  $T_{1ave}$  is determined at different pore fluid contents. If the surface area ( $A_s$ ) is constant, a plot of  $1/T_{1ave} - 1/T_{1b}$  versus  $M_v$  (determined gravimetrically) should be linear. In this work, three gels (35, 47, 55 wt% Al<sub>2</sub>O<sub>3</sub>) were cast in 25-mm NMR tubes and allowed to slowly dry at 303 K.  $M(\tau)$  was measured using a 90°- $\tau$ -90° pulse sequence with 32  $\tau$  points spaced at every 100 ms (every 75 ms for some samples with shorter  $T_1$  values). Measurements were made at a proton frequency of 10 MHz using a pulse spectrometer.<sup>†††</sup> The distribution of pore volume with  $T_1$  was found using a nonnegative least squares (NNLS) algorithm

described elsewhere<sup>11</sup> and the average  $T_1$  was found using the method given by Glaves and co-workers.<sup>10</sup>

Samples of the dried powders were loosely packed in 1-mm path-length cells for analysis by small-angle scattering. Small-angle X-ray scattering (SAXS) was performed at Sandia National Laboratories using 0.154-nm slit-collimated illumination<sup>†††</sup> and small-angle neutron scattering (SANS) was performed at the Missouri University Research Reactor using 0.475 nm point-collimated neutrons. The SAXS data were desmeared to remove the effects of slit collimation so that the SAXS and SANS data could be directly compared. The scattered intensity,  $I(q)$ , at a given scattering wave vector,  $q$  (where  $q = (4\pi/\lambda) \sin(\theta/2)$ , with  $\lambda$  the wavelength and  $\theta$  the scattering angle), reflects the scattering density fluctuations in the sample with the wave vector,  $q$ .

$$I(q) = \int g(r) \frac{\sin(qr)}{qr} 4\pi r^2 dr \quad (2)$$

where  $g(r)$  is the correlation function of density fluctuations.

Solid-state NMR provides information complementary to XRD since the technique is capable of determining the local environments of specific nuclei, regardless of sample homogeneity or degree of crystallinity. The technique has been successfully used to characterize aluminas,<sup>12–15</sup> silicates,<sup>14–16</sup> and aluminosilicates.<sup>17–19</sup> Natural abundance <sup>29</sup>Si and <sup>27</sup>Al magic-angle spinning nuclear magnetic resonance (MASNMR) spectra were acquired using a wide-bore instrument<sup>§§§</sup> equipped with a solids accessories<sup>¶¶¶</sup> and a 7.05 T cryomagnet operating at a proton resonance frequency of 300.1 MHz. The rotation angle was adjusted using the <sup>79</sup>Br resonance of KBr.<sup>20</sup> <sup>29</sup>Si spectra were acquired at 59.6 MHz using 45° (3.25  $\mu$ s) single-pulse excitation and high-power decoupling gated on during the acquisition time. A recycle time of 90 s was used to ensure quantitative analysis. Samples were contained in rotors<sup>\*\*\*\*</sup> and spun at 3 kHz. <sup>29</sup>Si chemical shifts were referenced to tetramethylsilane (TMS, (CH<sub>3</sub>)<sub>4</sub>Si). <sup>27</sup>Al spectra were acquired at 78.2 MHz using 1- $\mu$ s pulses (30° measured on Al(H<sub>2</sub>O)<sub>6</sub><sup>3+</sup>) and 1-s recycle delays. Samples were placed in rotors<sup>††††</sup> and spun at rotation rates of up to 8 kHz. Proton decoupling was not used because of the negligible contribution of dipolar broadening to the observed linewidths. <sup>27</sup>Al chemical shifts were referenced to aqueous Al(H<sub>2</sub>O)<sub>6</sub><sup>3+</sup>.

One set of four samples was prepared with compositions of 21, 47, 68, and 75 wt% Al<sub>2</sub>O<sub>3</sub> (dry basis) as determined via X-ray fluorescence (XRF). XRD analysis indicated that all four samples were amorphous. For the low-field NMR experiments, a second set of samples (35, 47, and 55 wt%) was synthesized as both powders and monoliths.

## III. Results

Figure 1 shows the nitrogen surface area as a function of the Al<sub>2</sub>O<sub>3</sub> content for the samples used in this work as well as those previously investigated.<sup>1</sup> As was previously observed, a large drop in accessible surface area is noted in the region of 47 wt% Al<sub>2</sub>O<sub>3</sub>. Although not shown in Fig. 1, numerous duplicate samples were synthesized at 47 wt%, and they all exhibited surface areas between 1 and 2 m<sup>2</sup>/g. Figure 2 shows the corresponding skeletal density (from helium displacement) as a function of Al<sub>2</sub>O<sub>3</sub> content. As noted previously,<sup>1</sup> a significant decrease in density is observed in the same compositional region as the low surface area samples.

Preliminary TEM images of the 21, 47, 68, and 75 wt% gels are presented in Fig. 3 to 6, respectively. The 21 wt% compo-

<sup>7</sup>No. 541, Whatman, Inc., Clifton, NJ.

<sup>8</sup>No. 1, Whatman, W. & R. Balston, Ltd., England.

<sup>9</sup>Triton X-100, Rohm and Haas Co., Philadelphia, PA.

<sup>\*\*</sup>Rigaku, Osaka, Japan.

<sup>††</sup>Scintag, Inc., Santa Clara, CA.

<sup>‡‡</sup>Autosorb 1, Quantachrome Corp., Syosset, NY.

<sup>§§</sup>Quantachrome Corp., Syosset, NY.

<sup>¶¶</sup>Model JEM-2000FX, JEOL, Ltd., Tokyo, Japan.

<sup>\*\*\*</sup>Model CM30ST, Philips Electronic Instruments, Inc., Mahwah, NJ.

<sup>†††</sup>PRAXIS, San Antonio, TX.

<sup>††††</sup>Rigaku.

<sup>§§§</sup>Model GN-300, General Electric Co., Fremont, CA.

<sup>¶¶¶</sup>Chemagnetics, Fort Collins, CO.

<sup>\*\*\*\*</sup>Kel-F, 3M, St. Paul, MN.

<sup>††††</sup>Torlon, Amoco Chemicals Corp., Chicago, IL.

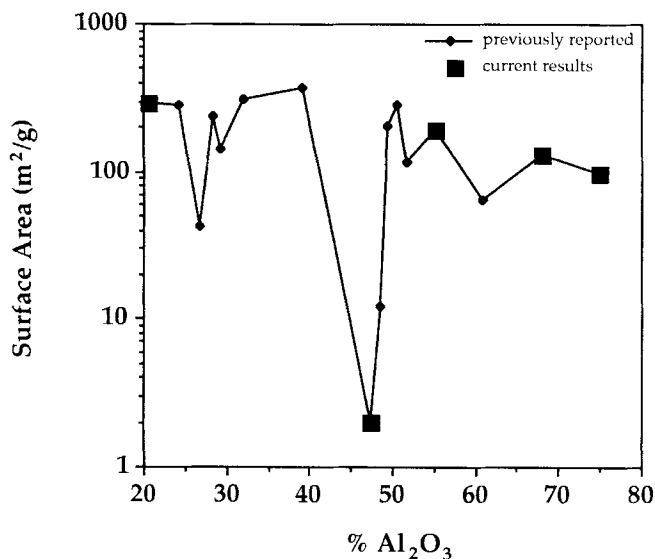


Fig. 1. Effect of Al<sub>2</sub>O<sub>3</sub> content on xerogel surface area.

sition clearly exhibits globular primary particles on the order of 10 nm in size, with a structure similar to that of base-catalyzed silica gels.<sup>24</sup> The 68 wt% sample also showed some evidence of this globular structure and contained occasional acicular crystallites of a few nm in size which exhibited lattice fringes (not evident in this micrograph). By comparison, the microstructure appeared considerably more uniform for the 47% and 75% samples.

Further examination of the 47 wt% powder by high-resolution microscopy at 300 kV showed a number of small, relatively equiaxed particulates as shown in Fig. 7. Clear lattice fringes are observed in these regions, which have dimensions on the order of 4 to 10 nm. In addition, bright-field/dark-field pairs that show these crystallites embedded within the primarily amorphous particles have been obtained. We suggest that these particles are the primary source of the observed neutron and X-ray scattering at length scales on the order of 5 nm, as discussed below. In the amorphous regions, deviation from the exact focus conditions allows the observation of a fine microstructure (see Fig. 8) which differs somewhat from the irregularly mottled appearance that is

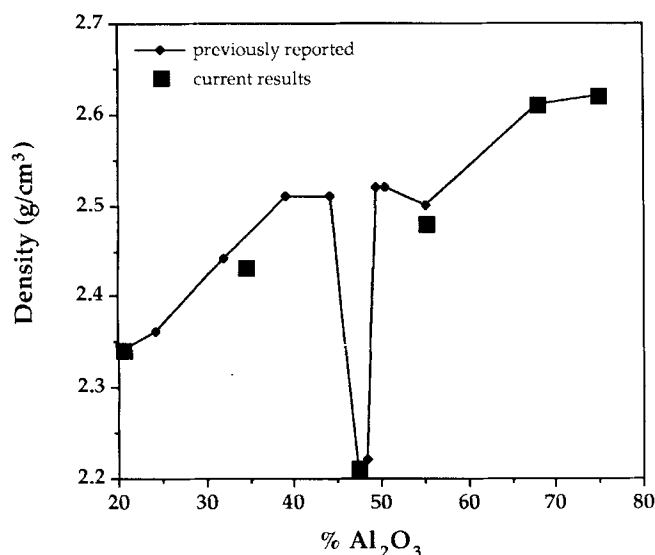


Fig. 2. Effect of Al<sub>2</sub>O<sub>3</sub> content on xerogel skeletal density (as determined via helium displacement).

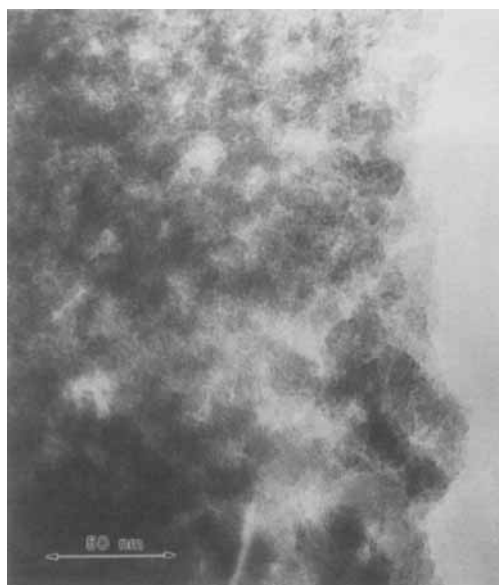


Fig. 3. HRTEM micrograph of 21 wt% Al<sub>2</sub>O<sub>3</sub> xerogel.

generally associated with fully dense amorphous materials. Bright, roughly circular spots (arrowed) may be indicative of pore structure on the 1 to 2 nm scale, although superposition of features along the beam direction makes quantitation difficult.

SAXS curves are presented in Fig. 9 for a range of compositions. The 47 wt% sample exhibits a structure which is qualitatively different from the other compositions. All samples exhibit a shoulder near  $1/q = 1$  nm, which could indicate small pores of that size (see Fig. 10 for smaller  $q$ ). The 47 wt% sample, which has only a suggestion of a peak at  $1/q = 1$  nm, exhibits larger scattering intensities at small  $q$ , near  $1/q = 5$  nm, possibly due to the microcrystals observed in high-resolution transmission electron microscopy (HRTEM).

SANS curves of two Al<sub>2</sub>O<sub>3</sub>-SiO<sub>2</sub> compositions are presented in Fig. 10. The SANS data cover smaller values of  $q$  and thus provide structural information on larger length scales. The 47 wt% sample exhibits a scattering intensity "shoulder" near  $1/q = 5$  nm, indicative of the microcrystals

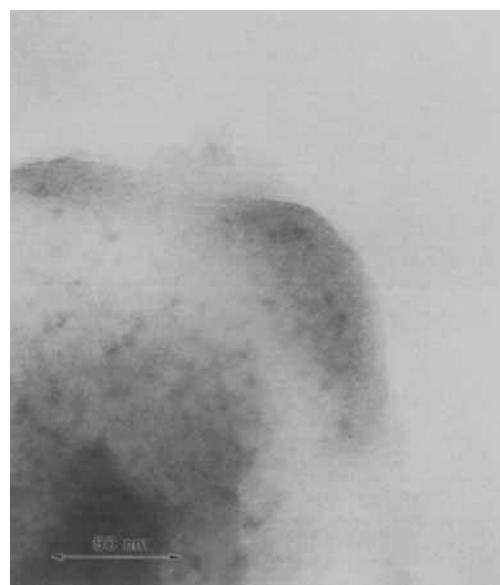


Fig. 4. HRTEM micrograph of 47 wt% Al<sub>2</sub>O<sub>3</sub> xerogel.



Fig. 5. HRTEM micrograph of 68 wt%  $\text{Al}_2\text{O}_3$  xerogel.

on the 5-nm length scale. The 68 wt% sample has no such feature in this  $q$  range (see Fig. 9 for larger  $q$ ). We cannot rule out the possibility that this 5-nm feature represents pores (scattering cannot differentiate the sign of the density fluctuations); however, such large pores should be obvious in TEM and they were not seen.

For the corresponding wet gels, unimodal  $T_1$  distributions of similar average  $T_1$  and distribution width were observed indicating similar initial pore-size distributions for these three samples. During the drying process, the gel shrinks until the matrix stiffens sufficiently such that upon further evaporation, the fluid-vapor meniscus penetrates the matrix. Since the analysis of relaxation data is more complicated during this second step of drying, the  $^1\text{H}$  NMR experiments were stopped when  $M_v$  ( $M_v$  is mass of solid gel/volume of solvent) had increased by a factor of 2 (i.e., the pore volume had decreased by a factor of 2). Therefore, these experiments provide information concerning differences in the initial pore structure of the gels and the first stage of drying. As given by



Fig. 6. HRTEM micrograph of 75 wt%  $\text{Al}_2\text{O}_3$  xerogel.



Fig. 7. Lattice fringes indicate the occasional presence of crystalline particles with dimensions of 4 to 10 nm in the 47 wt% alumina xerogel, as evident in this high-resolution electron micrograph.

Eq. (1), a plot of  $(1/T_{lave}) - (1/T_{1b})$  versus  $M_v$  should be linear for constant surface area and extrapolate through the origin. These plots are presented for the 35, 47, and 55 wt% samples in Fig. 11. The different values of  $M_v$  for a given sample correspond to different extents of drying. The data for the three gels are reasonably linear, and no significant differences are observed between samples. If the surface area of these wet gels actually varied by 2 orders of magnitude over this composition range (as indicated by nitrogen surface area of the dried xerogels), the 47 wt% gel would have a  $(1/T_{lave}) - (1/T_{1b})$  value of approximately zero for the  $M_v$  range studied. These results indicate that pore closure (or some other effect leading to low surface area) must occur during the final stages of drying ( $M_v/M_{v0} > 2$ ).

The  $^{27}\text{Al}$  MASNMR spectra of the aluminosilicate xerogels are shown in Figs. 12(A) to (D) as a function of  $\text{Al}_2\text{O}_3/\text{SiO}_2$  ratio. The sample rotation rate is sufficient to preclude any resonance interference arising from spinning sidebands. All spectra in Fig. 12 exhibit three resonances. The resonances at 58 and 0 ppm are indicative of tetrahedrally and octahedrally coordinated aluminum, respectively. The third resonance, at approximately 29 ppm, is consistent

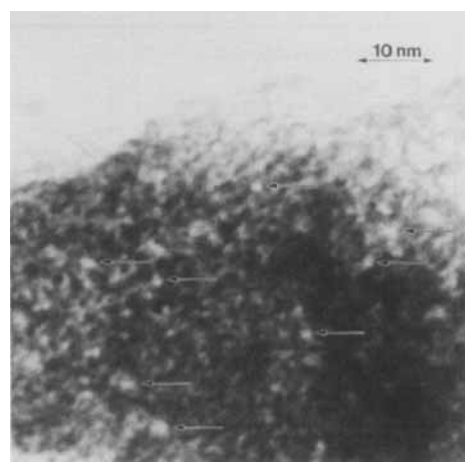


Fig. 8. HRTEM micrograph of the 47 wt% xerogel, obtained at a large defocus. Overall contrast variations are large, suggesting that contrast from nonuniformities through the sample thickness is superimposed on the mottled appearance generally observed for amorphous specimens. The bright dots observed in some locations may be indicative of pores with size of 1 to 2 nm.

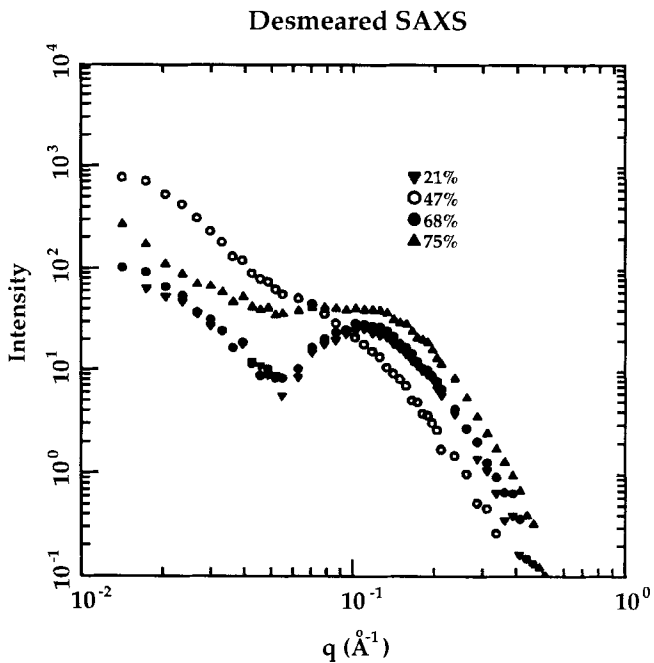


Fig. 9. Desmeared SAXS for 21, 47, 68, and 75 wt% Al<sub>2</sub>O<sub>3</sub> xerogels.

with the previously assigned<sup>22,23</sup> chemical shift of 5-coordinate aluminum. The large relative area of the resonance at 58 ppm in the 21 wt% sample (Fig. 12(A)) is consistent with the incorporation of a significant amount of aluminum into tetrahedral SiO<sub>2</sub> framework sites. The relative intensity of the 58 ppm resonance decreases noticeably as the Al<sub>2</sub>O<sub>3</sub>/SiO<sub>2</sub> ratio is increased to 47 wt% as shown in Fig. 12(B). Note that the relative intensities of the resonances due to 4- and 5-coordinate aluminum do not change significantly upon increasing the Al<sub>2</sub>O<sub>3</sub> ratio above 47 wt%. These observations suggest that a stepwise change in aluminum coordination occurs between 21 and 47 wt% Al<sub>2</sub>O<sub>3</sub>/SiO<sub>2</sub> since gradual changes in speciation are observed. All of the resonances in Fig. 12 have similar bandwidths, indicating that the short range order is independent of composition.

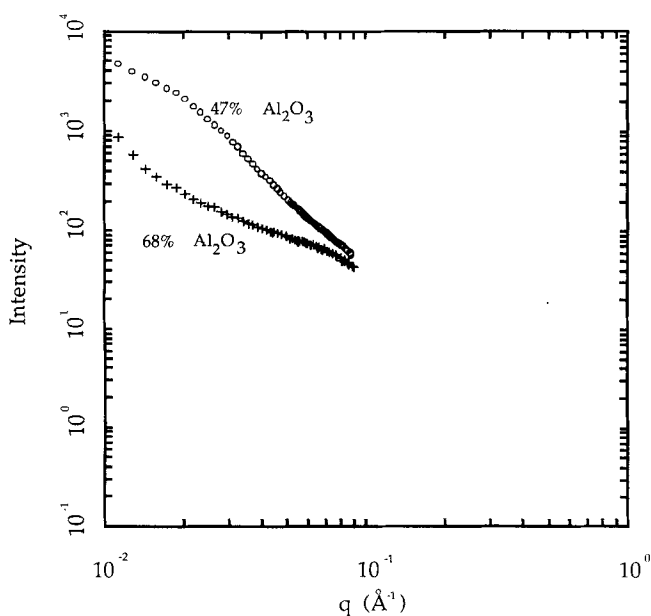


Fig. 10. SANS for 47 and 68 wt% Al<sub>2</sub>O<sub>3</sub> xerogels.

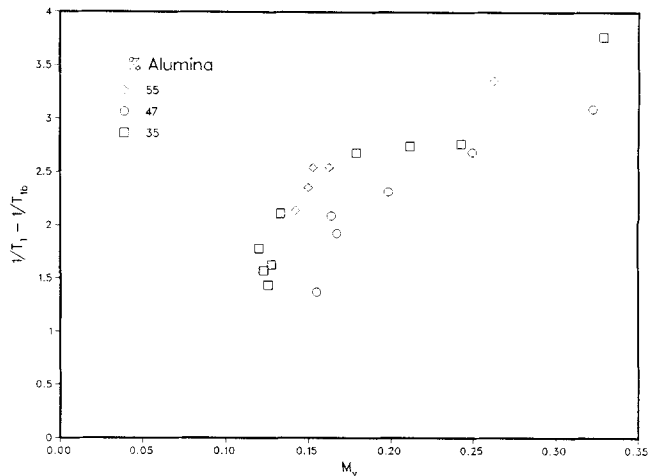


Fig. 11. Low-field NMR spin-lattice relaxation time as a function of fluid content during drying for 35, 47, and 55 wt% Al<sub>2</sub>O<sub>3</sub> gels.

The <sup>29</sup>Si MASNMR spectra of the aluminosilicate xerogels are shown in Figs. 13(B) to (D), as a function of the Al<sub>2</sub>O<sub>3</sub>/SiO<sub>2</sub> ratio. The <sup>29</sup>Si MASNMR spectrum of a pure SiO<sub>2</sub> gel is shown in Fig. 13(A) for comparison. All of the spectra exhibit one broad resonance, denoting a lack of crystallinity and indicating that a wide range of silicon environ-

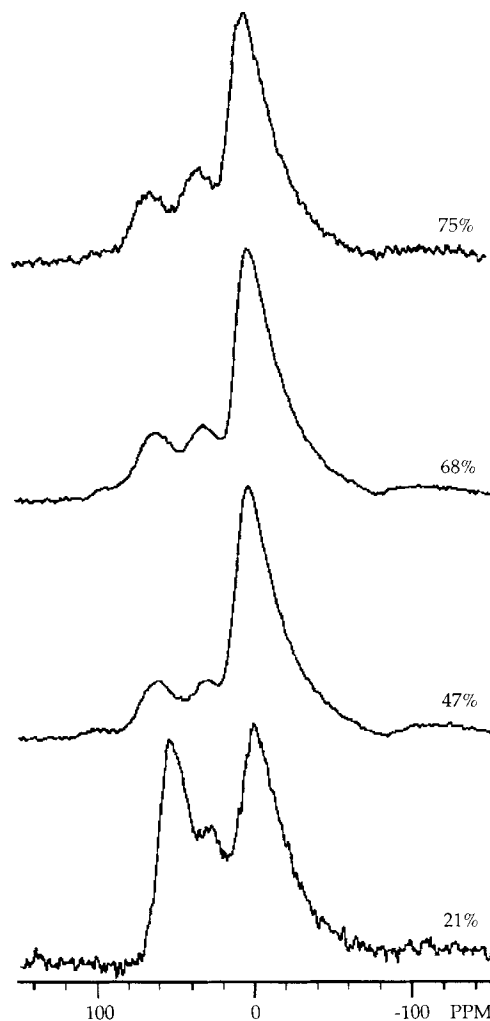


Fig. 12. <sup>27</sup>Al MASNMR spectra for 21, 47, 68, and 75 wt% Al<sub>2</sub>O<sub>3</sub> xerogels.

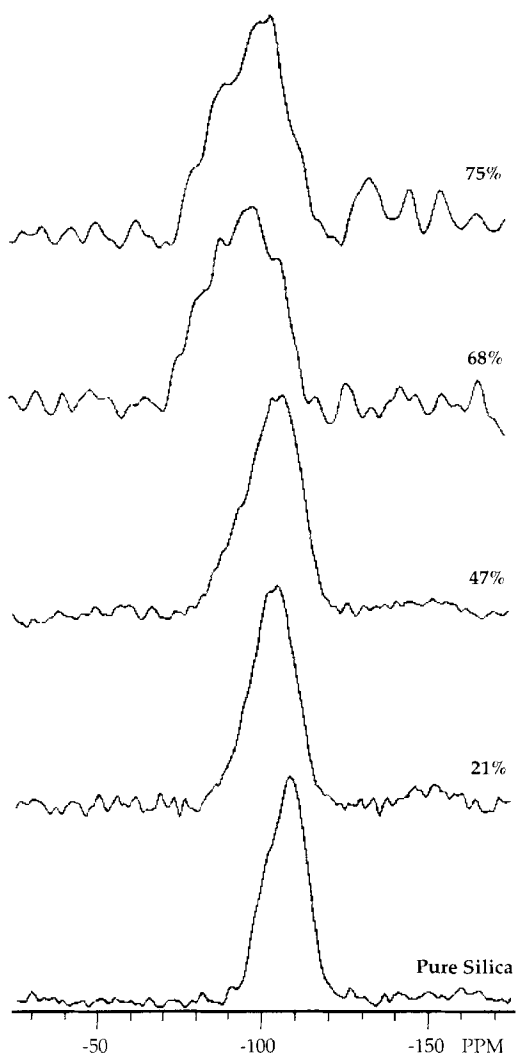


Fig. 13.  $^{29}\text{Si}$  MASNMR spectra for 0 (pure silica), 21, 47, 68, and 75 wt%  $\text{Al}_2\text{O}_3$  xerogels.

ments is present. The microcrystals observed in HRTEM are apparently too small and dilute to contribute a detectable signal. The lack of any well-defined peaks within the envelope of  $^{29}\text{Si}$  NMR resonances precludes any quantitative analysis of the silicon speciation.

The xerogel resonances broaden and shift slightly downfield, from  $-105$  to  $-98$  ppm, as the  $\text{Al}_2\text{O}_3/\text{SiO}_2$  ratio increases. This behavior is consistent with the progressive replacement of silicon with aluminum in the second coordinate sphere of silicon as the  $\text{Al}_2\text{O}_3$  content increases.<sup>12</sup> The observed chemical shift for the samples with high  $\text{Al}_2\text{O}_3$  concentrations ( $-98$  ppm) suggests that not all of the aluminum is incorporated into the silicate network and that a portion of aluminum exists in Al–O–Al bonds. This model would be consistent with the  $^{27}\text{Al}$  data discussed above, where, in addition to tetrahedrally coordinated aluminum, there is also penta- and hexa-coordinate aluminum.

Since the silicon/aluminum ratio corresponding to low surface area is approximately 1, (a composition which has been frequently studied for both catalysis and ceramics), it is surprising that this low surface area behavior has not been reported previously.<sup>2–9</sup> However, a review of the literature indicates that most of the previous studies used alcohol (or other low surface tension organic solvents) rather than water. Since pore closure appears to occur during drying, the pore fluid surface tension could affect the final surface area. To test this hypothesis, we prepared a second set of samples in which water was replaced with ethanol (by repeated washings)

prior to drying. The nitrogen surface areas for the ethanol-washed samples are compared with the standard water-washed samples in Table I. The effect of ethanol washing for the 47 wt% sample is dramatic and suggests that the reason this low surface area behavior has not been previously reported for the silicon/aluminum = 1 system is related to the use of water as the pore fluid. By comparison, for base-catalyzed  $\text{SiO}_2$  gels dried in either water or ethanol, a decrease in surface area on the order of 50% to 100% is noted when ethanol is replaced with water.<sup>25</sup> This difference compares favorably with our lowest  $\text{Al}_2\text{O}_3$  content sample (21 wt%). The effect of water may be related to its high surface tension and/or its effect on system chemistry.

In an attempt to separate surface tension and chemistry effects, a number of 47 wt% samples were prepared which had been washed in either water, ethanol, dioxane, formamide, water/surfactant, or ethanol followed by water. The surface area and pore volume for these samples are presented in Table II. The results in Table II indicate the expected trend of decreasing surface area and pore volume with increasing pore fluid surface tension. It appears that the effect of water is its high surface tension, since the water/surfactant pore fluid did not result in low surface area. To further probe the effect of surface tension, pore-size distributions (PSD) obtained from the desorption branch of nitrogen adsorption isotherms are presented in Fig. 14 for the ethanol-, water/surfactant-, and formamide-washed samples. Within the limits of our experimental precision, the water-washed sample has no accessible porosity. The ethanol sample exhibits a very sharp peak in the PSD at a pore radius of 2 nm. With increasing surface tension, the pore-size distribution decreases in magnitude (i.e., corresponding to a decrease in accessible pore volume at a given pore size) and broadens in pore size. All three samples exhibit significant microporosity as evidenced by the nonzero  $dV/d \log r$  at the lower pore-size limit.

#### IV. Conclusions

The results of high-resolution transmission electron microscopy (HRTEM), small-angle X-ray scattering (SAXS), and small-angle neutron scattering (SANS) are consistent with the presence of closed porosity in the 47 wt%  $\text{Al}_2\text{O}_3$  sample as an explanation for the low surface area and helium density observed in this composition. However, the results of X-ray diffraction (XRD) and the  $^{29}\text{Si}$  and  $^{27}\text{Al}$  nuclear magnetic resonance (NMR) do not provide clues as to the compositional dependence of the anomalous surface area/skeletal density behavior. If the effect of water on low surface area behavior is solely a result of high surface tension, one would not expect the effect to be observed over such a narrow range of composition.

We postulate that during the final stages of drying the 47 wt% composition, the pore structure of the wet gel is primarily microporous. The high capillary forces associated with the microporosity and water in the pores serves to form closed pores. The mechanism by which actual pore closure occurs may be the formation of small crystallites (of a high-pressure  $\text{SiO}_2/\text{Al}_2\text{O}_3$  phase) in the pore throats (which may or may not be related to crystallinity observed via HRTEM), the presence of platelike substructure, or the fact that the matrix at this composition is more compliant than other composi-

Table I. Effect of Pore Fluid on Xerogel Surface Area

$\text{Al}_2\text{O}_3$ (wt%)	Water washed ( $\text{m}^2/\text{g}$ )	Ethanol washed ( $\text{m}^2/\text{g}$ )
21	287	548
47	2	463
68	130	549
75	97	488

**Table II. Effect of Pore Fluid Surface Tension on Surface Area and Pore Volume for 47 wt% Xerogels**

Fluid*	$\sigma$ , (dyne/cm)	Surface area (m <sup>2</sup> /g)	Pore volume (cm <sup>3</sup> /g)	Reference
Water	73	0.42	0.004	26
Ethanol then water	73	1.2	0.005	26
Formamide	58	307.8	0.232	26
Dioxane	38	429.1	0.351	27
Ethanol	22	438.8	0.303	26
Water/surfactant	≈20	534.3	0.370	26

\*At room temperature.

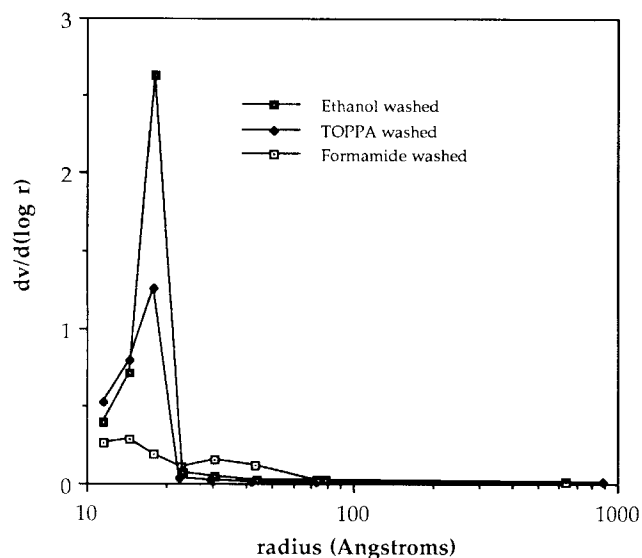


**Fig. 14.** Nitrogen desorption pore-size distributions for 47 wt% xerogels dried in different surface tension fluids.

tions. Reasons that the 47 wt% composition does not have large pores and the actual pore closure mechanism remain the object of further study.

**Acknowledgments:** The authors thank G. Johnston of the UNM/NSF Center for Micro-Engineered Ceramics (CMC) for performing the nitrogen adsorption measurements and P. Davis of CMC for conducting the low-field NMR measurements. Initial TEM work<sup>18</sup> was performed in the Electron Microbeam Analysis Facility in the Department of Geology and Institute for Meteoritics at the University of New Mexico. Additional TEM work was performed at the facility<sup>23</sup> located in, and used by courtesy of, the Center for Materials Science at Los Alamos National Laboratory.

## References

- S. L. Hietala, J. L. Golden, D. M. Smith, and C. J. Brinker, "Anomalous Low Surface Area and Density in the Silica/Alumina Gel System," *J. Am. Ceram. Soc.*, **72**, C-2354-C-2358 (1989).
- V. C. F. Holm, G. C. Bailey, and A. Clark, "Activity Studies of Silica-Alumina Catalysts," *J. Phys. Chem.*, **63**, 129-33 (1959).
- A. Clark, V. C. F. Holm, and D. M. Blackburn, "The Nature of Silica-Alumina Surfaces. 1. Thermodynamics of Adsorption of Ammonia," *J. Catal.*, **1**, 244-54 (1962).
- A. J. Leonard, P. Ratnasamy, F. D. Declerck, and J. J. Fripiat, "Structure and Properties of Amorphous Silico-Aluminas, Part-5—Nature and Properties of Silico-Alumina Surfaces," *Discuss. Faraday Soc.*, **52**, 98-108 (1971).
- P. G. Rouxhet and R. E. Sempels, "Hydrogen Bond Strengths and Acidities of Hydroxyl Groups on Silica-Alumina Surfaces and in Molecules in

Solution," *J. Chem. Soc. Faraday Trans.*, 2021-32, (1974).

<sup>6</sup>R. Roy and E. F. Osborn, "The System Al<sub>2</sub>O<sub>3</sub>-SiO<sub>2</sub>-H<sub>2</sub>O," *Am. Mineral.*, **39**, 853 (1954).

<sup>7</sup>J. H. DeBoer, "Constitution and Properties of Silica-Alumina Catalysts," *Discuss. Faraday Soc.*, **52**, 109-20 (1971).

<sup>8</sup>J. B. Moyer, N. N. Hughes, and R. C. Winterton, "Synthesis of Oxide Ceramic Powders by Aqueous Coprecipitation"; p. 117 in *Better Ceramics Through Chemistry, Vol. II*. Edited by C. J. Brinker, D. E. Clark, and D. R. Ulrich. Materials Research Society, Pittsburgh, PA, 1986.

<sup>9</sup>O. Johnson, "Acidity and Polymerization Activity of Solid Acid Catalysts," *J. Phys. Chem.*, **59**, 827 (1955).

<sup>10</sup>C. L. Glaves, C. J. Brinker, D. M. Smith, and P. J. Davis, "In Situ Pore Structure Studies of Xerogel Drying," *Chem. Mater.*, **1**, 34 (1989).

<sup>11</sup>K. Munn and D. M. Smith "A NMR Technique for the Analysis of Pore Structure: Numerical Inversion of Relaxation Measurements," *J. Colloid Interface Sci.*, **119**, 117 (1987).

<sup>12</sup>C. John, N. Alma, and G. Hayes, "Characterization of Transition Alumina by Solid-State Magic-Angle Spinning Aluminum NMR," *Appl. Catal.*, **6**, 341 (1983).

<sup>13</sup>J. Covino and R. Nissan, "Synthesis and Characterization of Aluminum Propionate Sol-Gel-Derived Al<sub>2</sub>O<sub>3</sub>," *Mater. Res. Bull.*, **21**, 377-44 (1986).

<sup>14</sup>E. Lippmaa, M. Magi, A. Samosan, G. Englehardt, and A. Grimmer, "Structural Studies of Silicates by High-Resolution <sup>29</sup>Si NMR," *J. Am. Chem. Soc.*, **102**, 4889 (1980).

<sup>15</sup>B. Sherriff and H. Grundy, "Calculations of <sup>29</sup>Si MAS NMR Chemical Shifts from Silicate Mineral Structure," *Nature (London)*, **332**, 819-22 (1988).

<sup>16</sup>J. Smith and C. Blackwell, "Nuclear Magnetic Resonance of Silica Polymorphs," *Nature (London)*, **303**, 223-25 (1983).

<sup>17</sup>E. Lippmaa, M. Magi, A. Samosan, M. Tarmak, and G. Englehardt, "Investigation of the Structure of Zeolites by High-Resolution <sup>29</sup>Si NMR Spectroscopy," *J. Am. Chem. Soc.*, **103**, 4992-96 (1981).

<sup>18</sup>J. Murdoch, J. Stebbins, and I. Carmichael, "High-Resolution <sup>29</sup>Si NMR Study of Silicate and Aluminosilicate Glasses. The Effect of Network-Modifying Cations," *A. Mineral.*, **66**, 678-70 (1985).

<sup>19</sup>S. Khomarneni, R. Roy, C. Fyfe, G. Kennedy, and H. Strobl, "Solid-State <sup>27</sup>Al and <sup>29</sup>Si Magic-Angle Spinning NMR of Aluminosilicate Gels," *J. Am. Ceram. Soc.*, **69**, C-42-C-44 (1986).

<sup>20</sup>J. Frye and G. Maciel, "Setting the Magic Angle Using a Quadrupolar Nucleus," *J. Magn. Reson.*, **48**, 125 (1982).

<sup>21</sup>V. Mastikhin, O. Krivoruchko, B. Zolotovskii, and R. Buyanov, "Study of Local Environment and Cation Distribution in Al(III) Oxides by <sup>27</sup>Al NMR with Sample Rotation at a 'Magic' Angle," *React. Kinet. Catal. Lett.*, **18**, 117-20 (1981).

<sup>22</sup>L. Alemany and G. Kirker, "First Observation of 5-Coordinate Aluminum by MAS <sup>27</sup>Al NMR in Well-Characterized Solids," *J. Am. Chem. Soc.*, **108**, 6158-62 (1986).

<sup>23</sup>A. Irwin, J. Holmgren, and J. Jonas, "<sup>27</sup>Al and <sup>29</sup>Si NMR Study of Sol-Gel-Derived Aluminosilicates and Sodium Aluminosilicates," *J. Mater. Sci.*, **23**, 2908 (1988).

<sup>24</sup>C. J. Brinker, W. D. Drotning, and G. W. Scherer, "A Comparison between the Densification Kinetics of Colloidal and Polymeric Silica Gels"; pp. 25-32 in *Better Ceramics Through Chemistry, Vol. I*, Edited by C. J. Brinker, D. E. Clark, and D. R. Ulrich. Materials Research Society, Pittsburgh, PA, 1984.

<sup>25</sup>P. J. Davis, C. J. Brinker, and D. M. Smith, "Pore Structure Evolution in Silica Gels During Aging"; unpublished work.

<sup>26</sup>CRC Handbook of Chemistry and Physics, 70th Ed.; pp. F35-F37. CRC Press, Boca Raton, FL, 1989.

<sup>27</sup>Lange's Handbook of Chemistry, 13th Ed.; p. 10-108. McGraw-Hill, New York, 1985. □